

# SPECTRA OF COHERENT TRANSMITTANCE AND REFLECTANCE OF PERIODIC, FIBONACCI, AND THUE-MORSE MULTILAYERS OF DIELECTRIC PARTICLES

A. A. Miskevich, V. A. Loiko

B.I. Stepanov Institute of physics of NAS of Belarus,  
68 Nezalezhnastsi ave., Minsk, 220072, Belarus  
miskevic@dragon.bas-net.by, loiko@dragon.bas-net.by

**PACS 78.67.Pt, 42.70.Qs, 61.44.-n, 68.65.Ac**

Coherent transmittance and reflectance of multilayers consisting of one-dimensional Fibonacci, Thue-Morse, and periodic sequences of plane-parallel ordered monolayers of spherical alumina and silica particles are investigated in the  $0.3 \mu\text{m}$  to  $2 \mu\text{m}$  spectral range. Consideration is based on the quasicrystalline approximation for individual monolayers and the transfer matrix method for multilayers. Comparison with sequences of the homogeneous plane-parallel layers is made. It is shown that the Fibonacci and Thue-Morse structures provide more possibilities to control light in comparison with the regular ones. These results can be used for the development of optical filters, solar cells, light emitting diodes, displays, etc.

**Keywords:** photonic crystal, non-periodic sequence, quasicrystalline approximation, transfer matrix method, coherent transmittance and reflectance.

## 1. Introduction. Statement of the problem

Currently, ordered structures, such as photonic crystals (PC) and quasicrystals (PQC) are the subject of intense research because they allow one to solve the problems concerning the control of spectral, temporal and spatial characteristics of light, and thus, to create new types of intensity, phase, and polarization modulators [1-21]. There is a set of natural biological systems which have ordered and quasi-ordered photonic crystal structures [22-24]. Great attention is paid to periodic and non-periodic ordered structures due to the photonic band gap effect [1-3]. Interest in the study of non-periodic ordered structures is caused by the additional possibilities (relative to periodic structures) to control the characteristics of transmitted and reflected light. For example, quasiperiodic PCs can be used to enhance the efficiency of light-emitting diodes [6]. Usually, Fibonacci (quasiperiodic) [10-16] and Thue-Morse (aperiodic) [16-17] sequences of the constituents are considered for such structures. Periodic structures possess the long-range order, while quasiperiodic and aperiodic photonic crystals display long-range and short-range orders.

The one-dimensional (1D) Fibonacci sequence  $L_n$  of symbols  $A$  and  $B$  is built according to the inflation rule  $L_n = L_{n-1}L_{n-2}$  (for  $n \geq 2$ , where  $n$  is the number of the sequence element), beginning from  $L_0 = A$  and  $L_1 = AB$ :  $L_0 = A$ ,  $L_1 = AB$ ,  $L_2 = ABA$ ,  $L_3 = ABAAB$ ,  $L_4 = ABAABABA, \dots$  The 1D Thue-Morse sequence  $L_n$  of symbols  $A$  and  $B$  is built according to the rule  $L_n = L_{n-1} \underline{L}_{n-1}$  (for  $n \geq 1$ , where  $\underline{L}_{n-1}$  element is “inverted”  $L_{n-1}$  element), beginning from  $L_0 = A$ :  $L_0 = A$ ,  $L_1 = AB$ ,  $L_2 = ABBA$ ,  $L_3 = ABBABAAB$ ,  $L_4 = ABBABAABBAABABBA, \dots$  The  $A$  and  $B$  symbols indicate sequence constituents with different properties.

Generally, sequences of homogenous layers are considered. The periodic (regular), Fibonacci, and Thue-Morse sequences of the homogeneous layers are schematically presented in Fig. 1. The symbols  $A$  and  $B$  in this figure indicate different layer types.

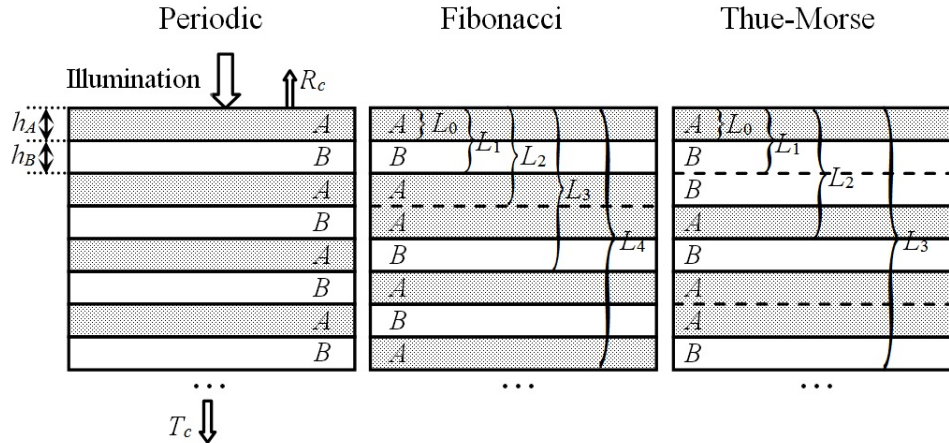


FIG. 1. Schematic representation of layered structures with the periodic (regular), Fibonacci, and Thue-Morse sequences consisting of  $A$  and  $B$  types of homogeneous layers (side view). With normal illumination,  $T_c$  and  $R_c$  are the coherent transmission and reflection coefficients, respectively, while  $h_A$  and  $h_B$  are the thicknesses of the  $A$  and  $B$  layer types, respectively. The dashed lines denote the “virtual interfaces” between the layers of the same type, and  $L_n$  are the sequence elements

The sequences of homogeneous layers are well studied theoretically and experimentally [25–28]. However, structures consisting of non-periodic sequences of particle monolayers have not been sufficiently investigated yet. Such structures provide a new means for photonics applications.

In this work, we investigate theoretical aspects of the spectra of coherent transmission and reflection coefficients of multilayers consisting of periodic, Fibonacci and Thue-Morse sequences of the plane-parallel monolayers of the monodisperse spherical dielectric particles. We consider multilayers consisting of alumina ( $\text{Al}_2\text{O}_3$ ) and silica ( $\text{SiO}_2$ ) particles monolayers because these materials are widely used in photonic and optoelectronic devices. The schematic representation of such structures is given in Fig. 2.

It is worth noting that generally, monolayers are mutually independent and can be shifted along the dashed lines depicted in Fig. 2.

The spectral dependences of the real part of the  $\text{Al}_2\text{O}_3$  and  $\text{SiO}_2$  refractive indices  $n(\lambda)$  ( $\lambda$  is the wavelength of the incident light) are shown in Fig. 3 [29]. The imaginary parts of the refractive indices in this spectral range for both materials are zero.

## 2. Coherent transmittance and reflectance of monolayer. Basic equations

We use the quasicrystalline approximation (QCA) [30–34] of the statistical theory of the multiple scattering of waves [30,35–36] to calculate the coherent transmission  $T_c$  and reflection  $R_c$  coefficients of the monolayer of particles. We write them as follows [31–34]:

$$T_c = |t_c|^2 = \left| 1 - \frac{\eta}{x^2} \sum_{j=1}^N (2j+1)(z_j + y_j) \right|^2, \quad (1)$$

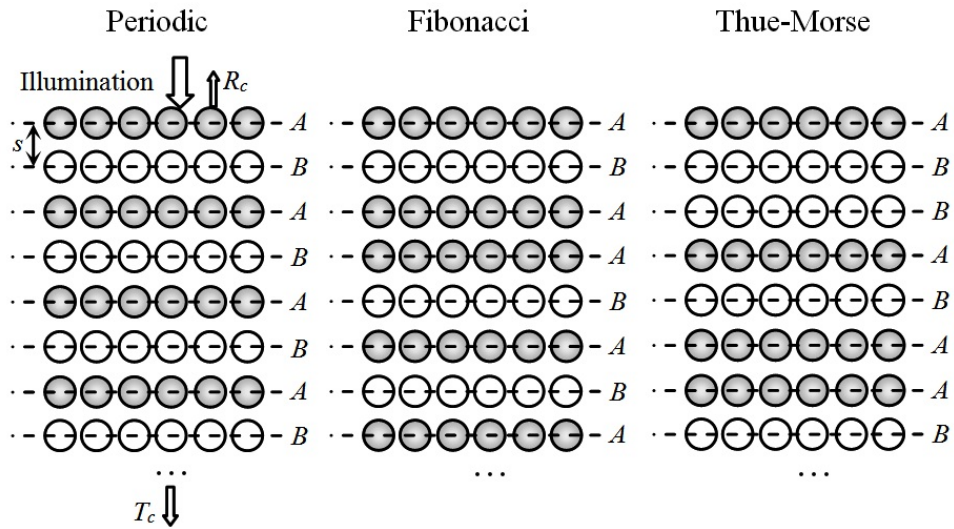


FIG. 2. Schematic representation of the layered structures consisting of the periodic (regular), Fibonacci, and Thue-Morse sequences of particulate monolayers of type  $A$  and type  $B$  (side view). Illumination is normal to the monolayers planes depicted by the dashed lines.  $T_c$  and  $R_c$  are the coherent transmission and reflection coefficients, respectively;  $s$  is the spacing between the adjacent monolayers

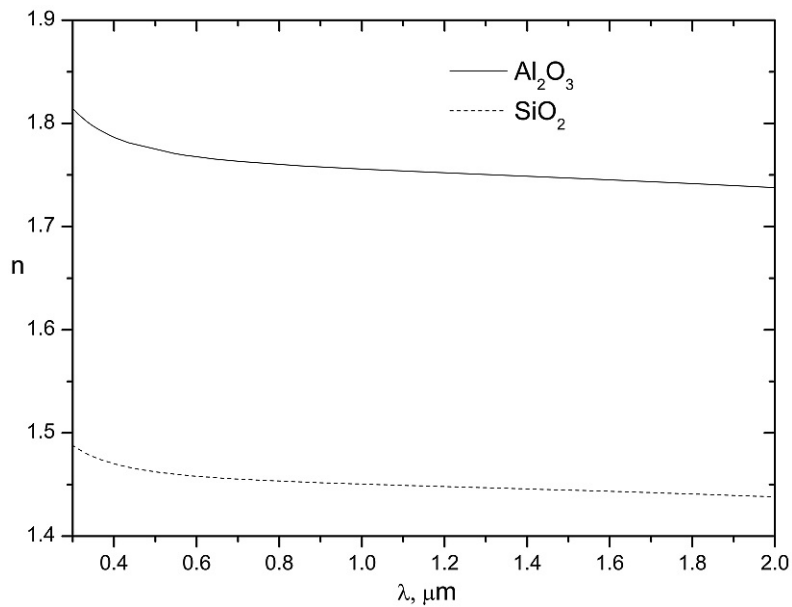


FIG. 3. Spectral dependences of the refractive index  $n$  of  $\text{Al}_2\text{O}_3$  and  $\text{SiO}_2$

$$R_c = |r_c|^2 = \left| -\frac{\eta}{x^2} \sum_{j=1}^N (-1)^j (2j+1) (z_j - y_j) \right|^2. \quad (2)$$

Here,  $t_c$  and  $r_c$  are the amplitude coherent transmission and reflection coefficients, respectively,  $\eta$  is the monolayer filling coefficient (the area fraction of the monolayer determined as the ratio of the projection areas of all particles to the area, where they are located),  $x = \pi D/\lambda$  is the size parameter of particle with diameter of  $D$ ,  $\lambda$  is the wavelength of the incident light,  $N = x + 4.05x^{1/3} + 2$  is the number of terms of the scattering series [37]. The  $z_j$  and  $y_j$  coefficients are found from the solution of the system of equations:

$$\begin{cases} z_l = b_l + \rho_0 b_l \sum_{j=1}^N (A_{lj} z_j + B_{lj} y_j) \\ y_l = a_l + \rho_0 a_l \sum_{j=1}^N (A_{lj} y_j + B_{lj} z_j) \end{cases}, \quad (3)$$

where  $a_l$  and  $b_l$  are the Mie coefficients for the particle size parameter  $x$  and complex refractive index  $m = n + i\kappa$ ,  $\rho_0$  is the averaged particle concentration in monolayer. The coefficients  $A_{lj}$  and  $B_{lj}$  are found from the solution of equations:

$$\begin{aligned} A_{lj} &= \frac{2j+1}{2} [l(l+1)j(j+1)]^{-\frac{1}{2}} \times \\ &\times \sum_{p=0,2,\dots}^N i^{-p} (2p+1) [l(l+1) + j(j+1) - p(p+1)] P_p(0) \times \\ &\times \begin{pmatrix} l & j & p \\ 0 & 0 & 0 \end{pmatrix} \begin{pmatrix} l & j & p \\ 1 & -1 & 0 \end{pmatrix} H_p, \end{aligned} \quad (4)$$

$$\begin{aligned} B_{lj} &= \frac{2j+1}{2} [l(l+1)j(j+1)]^{-\frac{1}{2}} \times \\ &\times \sum_{p=0,2,\dots}^N i^{-p} (2p+1) [(p+l-j)(p-l+j)(l+j+1+p)(l+j+1-p)]^{\frac{1}{2}} P_p(0) \times \\ &\times \begin{pmatrix} l & j & p-1 \\ 0 & 0 & 0 \end{pmatrix} \begin{pmatrix} l & j & p \\ 1 & -1 & 0 \end{pmatrix} H_p, \end{aligned} \quad (5)$$

$$H_p = 2\pi \int_D^\infty g(R) h_p^{(1)}(kR) R dR. \quad (6)$$

Here,  $g(R)$  is the radial distribution function [38-39],  $h_p^{(1)}(x)$  is the spherical Hankel function of the first kind and  $p$ -th order,  $k = 2\pi/\lambda$  is the wavenumber,  $\begin{pmatrix} j_1 & j_2 & j_3 \\ m_1 & m_2 & m_3 \end{pmatrix}$  is the Wigner  $3j$ -symbol [40]. To solve Eq. (6), we use the methods described in [31-34].

In the QCA, the coefficients  $T_c$  and  $R_c$  are determined by the sum of waves scattered by the particles, taking into account their re-illumination and correlation in their spatial locations. The correlation is described by the radial distribution function (RDF), which characterizes the probability of any particle's location in space relative to another one. There is a problem of calculating the RDF at high ordering of particles to make it applicable for the QCA. Recently, we proposed one of the solutions to this problem. We developed a method of calculating the RDF of a near-to-regularly-packed monolayer of spherical particles [33,34]. Such a monolayer represents the planar photonic crystal (PPC) [41-43]. To calculate the RDF of the PPC, we select the center of any particle as the coordinate origin and compute radii of the coordination circles [38,33,34] of the ideal crystal lattice and the number of particle centers for each circle. The distance dependence of the number of particle centers in

an ideal lattice is a set of the infinitely narrow peaks at distances equal to the coordination circle radii. Accordingly, the RDF of such a lattice has nonzero values at these distances and zero otherwise. Actual crystals typically have a nonideal lattice with coordination circles “blurred” into the “rings” with the fuzzy edges. Consequently, the peaks of the RDF are blurred as well. We showed [33,34] that the expression for the RDF  $g(u)$  of the near-to-regularly-packed monolayer can be written as:

$$g(u) = \rho_0^{-1} \sum_i \frac{N_i}{2\pi R_i} \frac{1}{\sqrt{2\pi}\sigma(u)} \exp\left(-\frac{(u - R_i)^2}{2\sigma^2(u)}\right). \quad (7)$$

Here,  $\sigma(u)$  is a blurring function that characterizes the broadening of the peaks with distance  $u$ . It is reasonable to use the linear blurring function:

$$\sigma(u) = \sigma_0(au + b). \quad (8)$$

In Eqs. (7) and (8),  $u = R/D$  is the dimensionless distance, expressed in particle diameters  $D$  ( $u \geq 1$ );  $R$  is the distance in a monolayer plane relative to the coordinate origin (see Eq. (6));  $\rho_0$  is the averaged numerical particle concentration in the monolayer;  $N_i$  is the number of particle centers on the coordination circle with radius  $R_i$  of an ideal crystal. The ordering degree and the scale of spatial order of the simulated crystals are specified by changing of  $\sigma_0$ , and the  $a$  and  $b$  coefficients, respectively. Equation (7) takes into account the asymmetry of the RDF's individual peaks, which are observed experimentally. This allows us to calculate the RDFs of the PCs in a wide range of their ordering degrees. The RDF obtained with Eq. (7) and Eq. (8) is well adapted for utilization in the QCA. The calculation of such a RDF and, consequently, coherent transmission and reflection coefficients of the PPC in the QCA, is fast and requires low amount of computational resources. The RDF of a highly ordered crystal is a sequence of narrow peaks at small  $u = R/D$  values (i.e. in the region near to the coordinate origin). With increased  $u$ -values, the peaks become wider, the function oscillates and converges to unity. Note that at  $\sigma(u)=\text{const}$ , Eq. (7) transforms into the known expression which describes the Gaussian blurring of peaks [39].

To obtain the RDF of the partially-ordered particle monolayers, we use the solution of the Ornstein-Zernike integral equation [44]. We numerically calculate it in the Percus-Yevick approximation [45] for a system of hard spheres by the iteration method [46]. Note that this function is deduced from the Poisson statistics while taking into account the finite particle size [46,47].

Figure 4 depicts the calculated spectra of the coherent transmission  $T_c$  and reflection  $R_c$  coefficients and their sum ( $T_c + R_c$ ) for monolayers with nonideal triangular particle lattice and for partially-ordered monolayers. The RDF of the monolayer with a triangular lattice is calculated using the blurring function  $\sigma(u) = \sigma_0 u$  at  $\sigma_0 = 0.01$ , while the filling coefficient of monolayers is  $\eta = 0.5$ , diameter of particles is  $D = 0.3 \mu\text{m}$ .

The plots display the influence that the spatial ordering of particles in the monolayer has on coherent transmission and reflection coefficients. At wavelengths comparable with the particle size, spectra of the regularly-packed monolayers have the sharp peaks caused by periodicity in the particle locations. For  $\lambda \geq 0.35 \mu\text{m}$ , the  $T_c + R_c$  sum of the regularly-packed monolayers is unity (see Fig. 4c). At these wavelengths, practically all radiation transmits straight through the monolayers and reflects straight back. This means that the incoherent (diffuse) component [46] of radiation is negligible. The  $T_c + R_c$  sum of the partially-ordered monolayers monotonically increases from  $\lambda \approx 0.41 \mu\text{m}$  (for monolayer of  $\text{SiO}_2$  particles) and

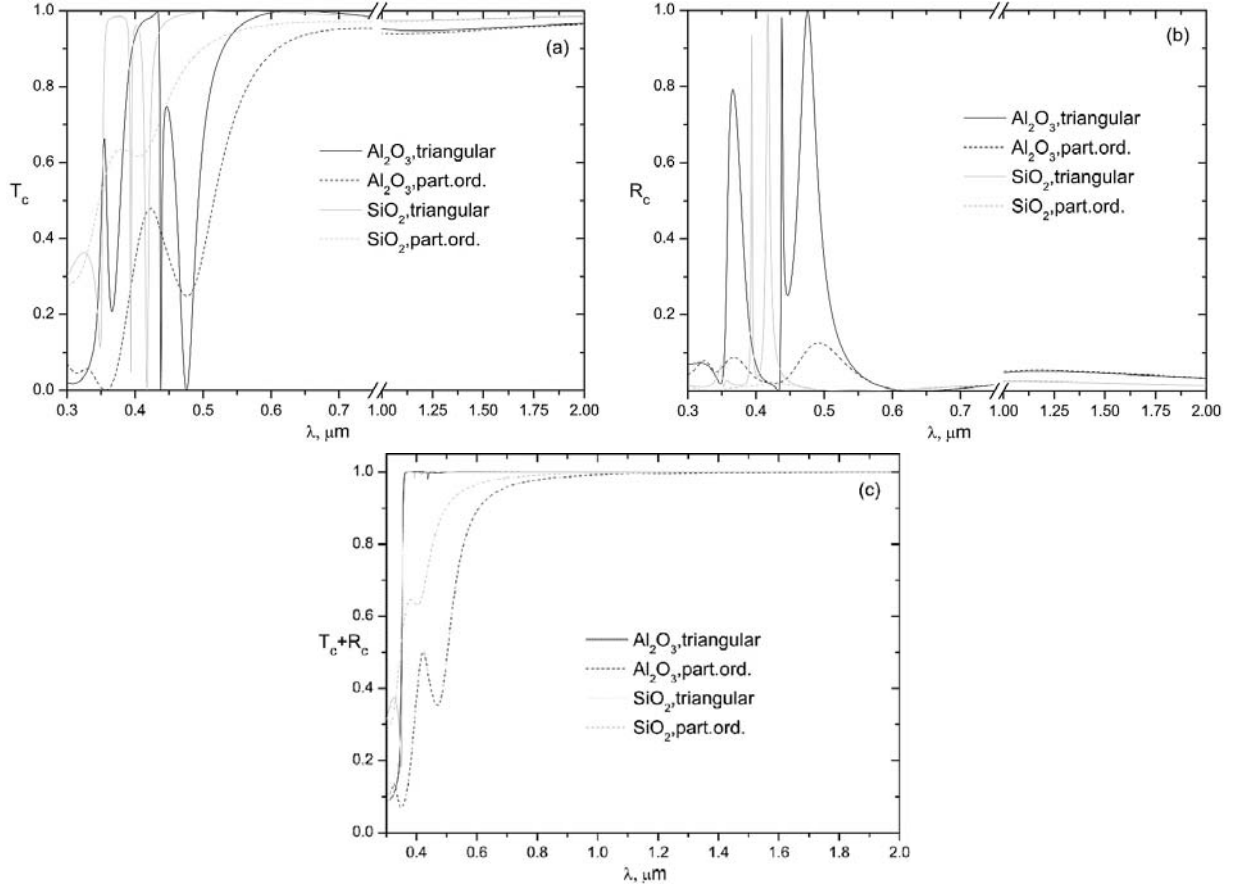


FIG. 4. Spectral dependence of the coherent transmission  $T_c$  (a) and reflection  $R_c$  (b) coefficients and their sum  $T_c + R_c$  (c) of the individual monolayers with a triangular lattice (solid lines) of monodisperse spherical  $\text{Al}_2\text{O}_3$  (black lines) and  $\text{SiO}_2$  (gray lines) particles and the partially-ordered monolayers (dashed lines) of the same particles. Diameter of particles is  $D=0.3\mu\text{m}$ . Filling coefficient of monolayers is  $\eta=0.5$ .  $\sigma(u) = \sigma_0 u$  at  $\sigma_0=0.01$

from  $\lambda \approx 0.5 \mu\text{m}$  (for a monolayer of  $\text{Al}_2\text{O}_3$  particles) and tends to unity with increased wavelength.

### 3. Transmittance and reflectance of a multilayer structure

#### 3.1. Basic equations

The amplitude coherent transmission  $t_c$  and reflection  $r_c$  coefficients obtained in the QCA for individual monolayers [see Eqs.(1),(2)] are used to calculate coherent transmission and reflection coefficients of the multilayer under the transfer matrix method (TMM) [25–27]. We consider the monolayers as interfaces and the spaces between them as the layers. Under the TMM, the amplitude coherent transmission  $t$  and reflection  $r$  coefficients of a multilayer can be written as follows [25,27]:

$$t = \frac{1}{T_{11}}, \quad (9)$$

$$r = \frac{T_{21}}{T_{11}}, \quad (10)$$

where  $T_{ij}$  are elements of the transfer matrix  $\mathbf{T}$  of the multilayer. For a system of  $N$  interfaces the transfer matrix  $\mathbf{T}$  can be written as [25,27]:

$$\mathbf{T}_{0,N} = \begin{bmatrix} T_{11} & T_{12} \\ T_{21} & T_{22} \end{bmatrix} = \begin{bmatrix} \frac{1}{t_{0,N}} & \frac{-r_{N,0}}{t_{0,N}} \\ \frac{r_{0,N}}{t_{0,N}} & \frac{t_{0,N}t_{N,0}-r_{0,N}r_{N,0}}{t_{0,N}} \end{bmatrix}. \quad (11)$$

Here,  $t_{0,N}$  and  $r_{0,N}$  are the amplitude coherent transmission and reflection coefficients of the multilayer for the forward propagating wave,  $t_{N,0}$  and  $r_{N,0}$  are the amplitude coherent transmission and reflection coefficients of the multilayer for the backward propagating wave.

The transfer matrix of a multilayer is calculated by the sequential multiplication of the transfer matrices of interfaces  $\mathbf{T}_j$  with the propagation matrices of the layers  $\mathbf{P}_j$ :

$$\mathbf{T}_{0,N} = \left( \prod_{j=1}^{N-1} \mathbf{T}_j \mathbf{P}_j \right) \mathbf{T}_N, \quad (12)$$

where

$$\mathbf{T}_j = \begin{bmatrix} \frac{1}{t_{j-1,j}} & \frac{-r_{j,j-1}}{t_{j-1,j}} \\ \frac{r_{j-1,j}}{t_{j-1,j}} & \frac{t_{j-1,j}t_{j,j-1}-r_{j-1,j}r_{j,j-1}}{t_{j-1,j}} \end{bmatrix}, \quad (13)$$

is the matrix of  $j$ -th interface,

$$\mathbf{P}_j = \begin{bmatrix} \exp(-ik_j h_j) & 0 \\ 0 & \exp(ik_j h_j) \end{bmatrix}, \quad (14)$$

is the propagation matrix of  $j$ -th layer,  $t_{j-1,j}$  and  $r_{j-1,j}$  are the amplitude coherent transmission and reflection coefficients of  $j$ -th interface for the forward propagating wave;  $t_{j,j-1}$  and  $r_{j,j-1}$  are the amplitude coherent transmission and reflection coefficients of  $j$ -th interface for the backward propagating wave (we calculate these coefficients in the QCA, see Eqs. (1),(2)); the wave number is  $k_j=2\pi m_j/\lambda$ ,  $m_j$  and  $h_j$  are the complex refractive index and thickness of  $j$ -th layer, respectively.

The energy coherent transmission  $T_c$  and reflection  $R_c$  coefficients of the multilayer are the squares of the absolute values of the amplitude coefficients:

$$T_c = |t|^2 = \left| \frac{1}{T_{11}} \right|^2, \quad (15)$$

$$R_c = |r|^2 = \left| \frac{T_{21}}{T_{11}} \right|^2. \quad (16)$$

### 3.2. Spectra of structures with different number of monolayers

Let us consider multilayers with different number of monolayers arranged in different sequences. Under the approach used, we study only the coherent component of radiation. That is why we restrict our consideration to the spectral range where the incoherent (diffuse) component is negligible.

Figure 5 depicts the spectra of the coherent transmission and reflection coefficients of the multilayers consisting of monolayers arranged in the regular, Fibonacci, and Thue-Morse sequences. The individual monolayers have the nonideal triangular lattice of monodisperse spherical  $\text{Al}_2\text{O}_3$  and  $\text{SiO}_2$  particles with a filling coefficient  $\eta=0.9$ . The spacing  $s$  (see Fig. 2) between the adjacent monolayers is  $0.3 \mu\text{m}$ . These parameters correspond to the three-dimensional (3D) ordered disperse structure, which is similar to the structure of the colloidal crystal. The symbols  $A$  and  $B$  denote the monolayer of  $\text{Al}_2\text{O}_3$  and  $\text{SiO}_2$  particles, respectively.

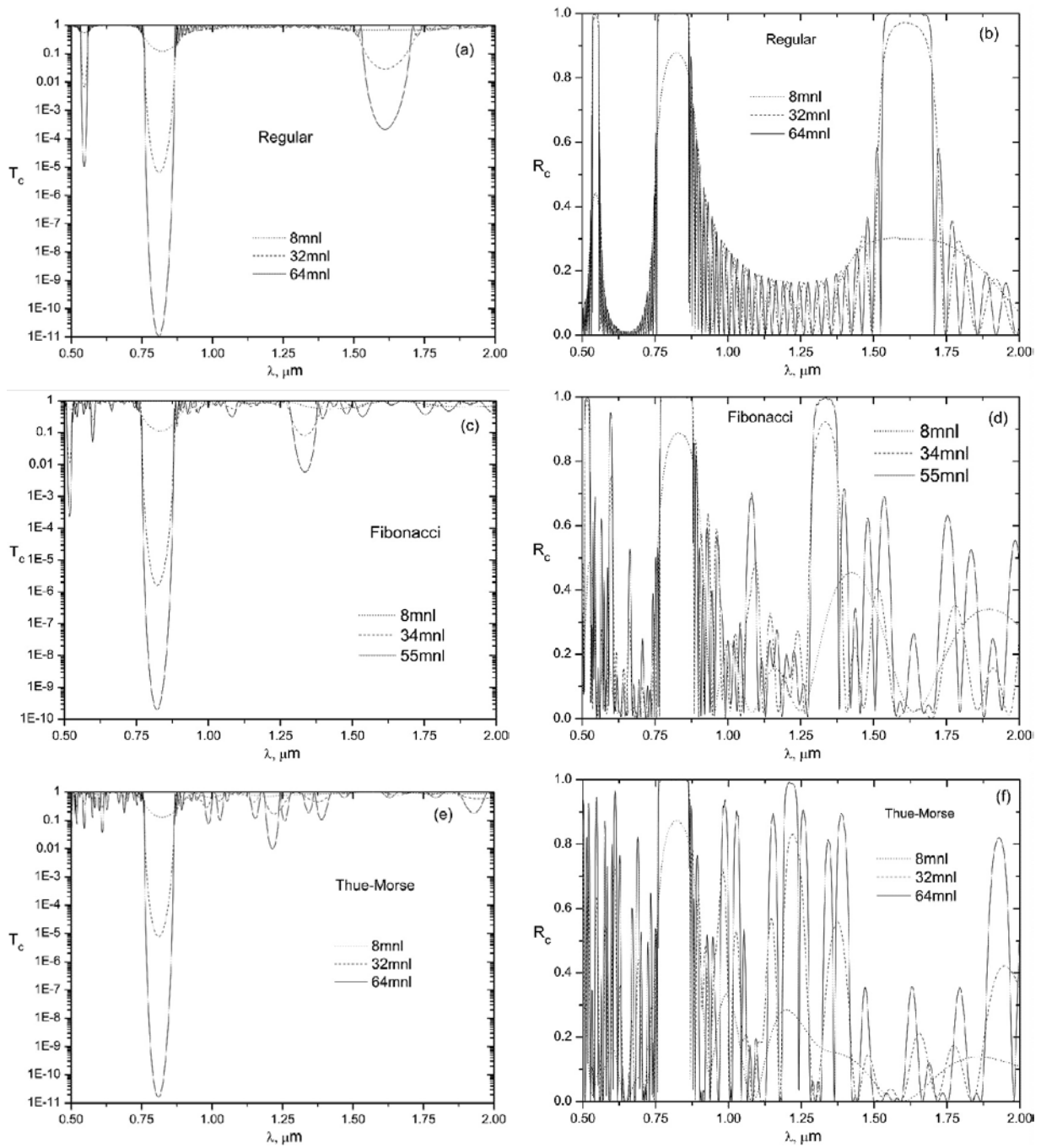


FIG. 5. Spectra of coherent transmission  $T_c$  (a),(c),(e) and reflection  $R_c$  (b),(d),(f) coefficients of the multilayer consisting of regular (a),(b), Fibonacci (c),(d), and Thue-Morse (e),(f) sequences of monolayers with a triangular lattice of monodisperse spherical  $\text{Al}_2\text{O}_3$  (type A) and  $\text{SiO}_2$  (type B) particles. Diameter of particles is  $D=0.3 \mu\text{m}$ . Filling coefficient of monolayers is  $\eta=0.9$ . The number of monolayers is 8, 32, 64 (a),(b),(e),(f), and 8, 34, 55 (c),(d). Blurring function is  $\sigma(u) = \sigma_0 u$ ,  $\sigma_0=0.001$ . Spacing between adjacent monolayers is  $s=0.3 \mu\text{m}$

As follows from the presented results, with an increased number of monolayers, photonic band gaps (PBGs) occur in the spectra of all considered sequences. In the spectrum of the regular sequence the one “main” and two “secondary” PBGs occur. They are caused by the regularity of the alternating monolayers of  $A$  and  $B$  types. The “main” PBG is observed in the wavelength range from  $0.76 \mu\text{m}$  to  $0.86 \mu\text{m}$ . The spectra of multilayers with Fibonacci and Thue-Morse sequences are more complicated. The “main” PBGs of their spectra occur practically in the same wavelength range as for the regular sequence. As one can see from Fig. 5(c),(e), the number of PBGs increases with an increased number of monolayers.

### 3.3. The PBG at different particle materials and filling coefficients of the adjacent monolayers

Let us consider the formation of the “main” PBG in more detail. Figure 6 depicts the coherent transmittance spectra of the layered structures consisting of 34 monolayers arranged in periodic, Fibonacci, and Thue-Morse sequences. This number of monolayers corresponds to the  $L_7$  element of the Fibonacci sequence. The influence of the differences between the  $A$ - and  $B$ -type monolayers on the transmittance spectra of the multilayer is shown. Different particle materials [Fig. 6(a)] and different filling coefficients [Fig. 6(b)] are considered. The spacing  $s$  between adjacent monolayers is  $0.3 \mu\text{m}$ , diameter of particles is  $D=0.3 \mu\text{m}$ .

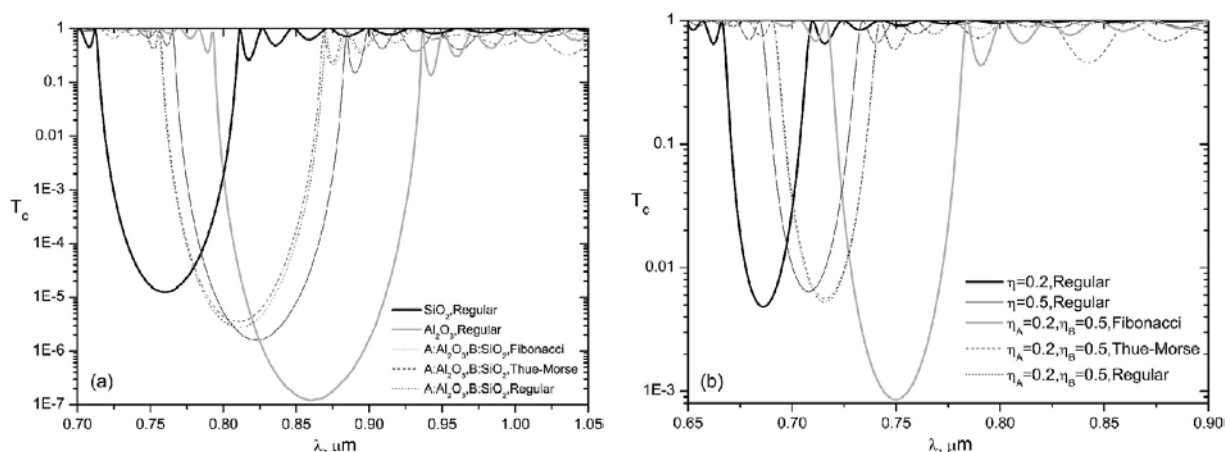


FIG. 6. Transmittance spectra of the layered structures of 34 monolayers arranged in regular, Fibonacci, and Thue-Morse sequences.  $D=0.3 \mu\text{m}$ ,  $s=0.3 \mu\text{m}$ , triangular lattice. (a) sequences of monolayers of  $\text{Al}_2\text{O}_3$  (type  $A$ ) and  $\text{SiO}_2$  (type  $B$ ) particles with  $\eta=0.9$ ;  $\sigma(u) = \sigma_0 u$ ,  $\sigma_0=0.001$ . (b) sequences of monolayers of  $\text{Al}_2\text{O}_3$  particles with  $\eta_A=0.2$  (type  $A$ ),  $\eta_B=0.5$  (type  $B$ );  $\sigma(u) = \sigma_0 u$ ,  $\sigma_0=0.01$

The results show that the PBG for the multilayer structure consisting of both  $A$ - and  $B$ -type monolayers is located between spectral positions of the PBGs for the multilayers composed of only type  $A$  and only type  $B$  monolayers.

### 3.4. Spectra of particulate and homogeneous multilayers

The monolayer of particles and the homogeneous layer are different in their structure. The first one has more structural parameters (such as concentration of particles, their shape, size distribution, type of spatial arrangement, etc.), which enhance the potentialities of the layered particulate structure.

Compare the spectra of the multilayer consisting of the plane-parallel homogeneous layers (see Fig. 1) with those of the multilayer consisting of the particulate monolayers (Fig. 2). Consider the influence of particle concentration and spacing between monolayers on the spectra in two cases: (i) the individual particulate and homogeneous layers have the same material volume, (ii) the individual particulate and homogeneous layers have the same thickness.

Figure 7 depicts the coherent transmittance spectra of the multilayers of  $\text{SiO}_2$  particles with different filling coefficients. The monolayers (type *A*) and spacings (type *B*) between them form the regular (Fig. 7a), Fibonacci (Fig. 7b), and Thue-Morse (Fig. 7c) multilayer structures.

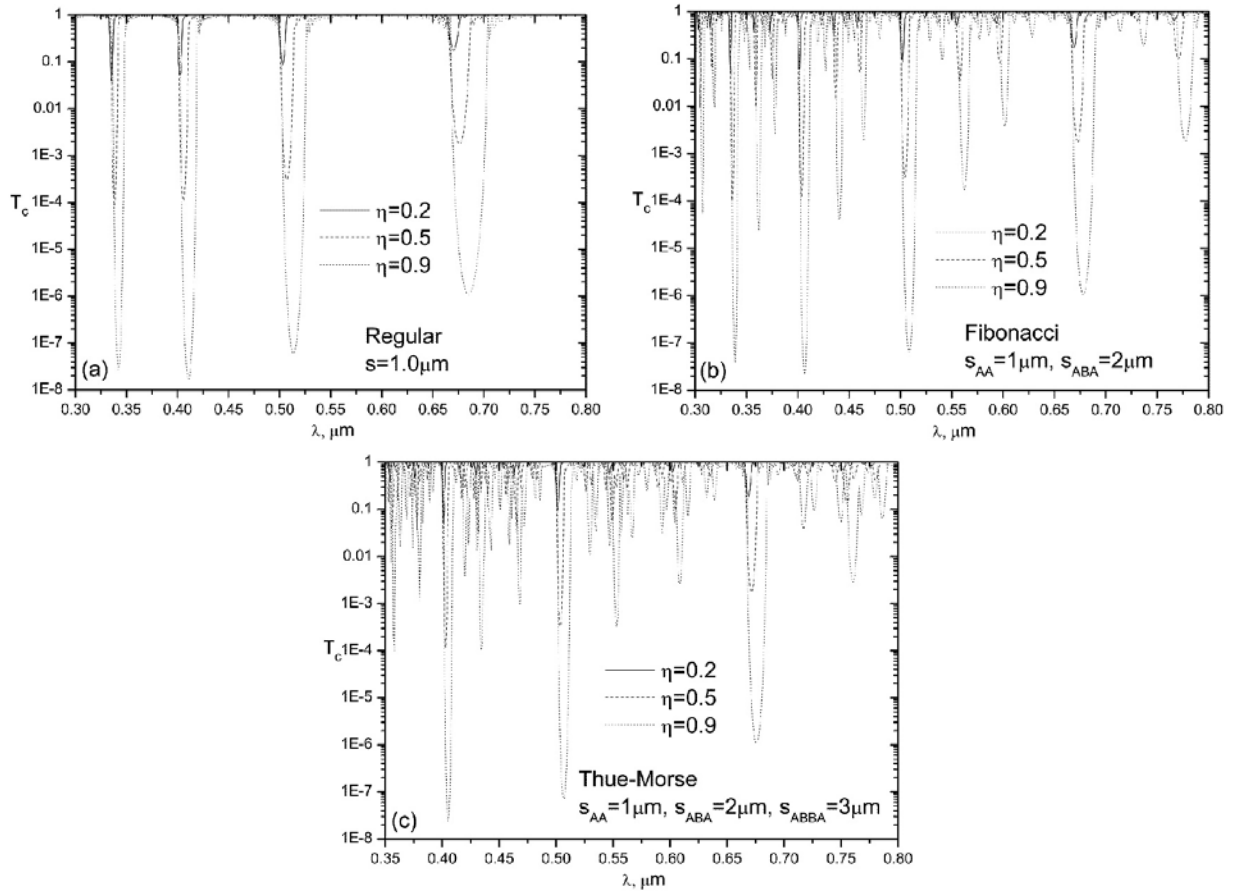


FIG. 7. The coherent transmittance spectra of the multilayers consisting of regular (a), Fibonacci (b), and Thue-Morse (c) sequences of monolayers at different filling coefficient  $\eta$ . The number of monolayers is 32. Individual monolayers (type *A*) have a triangular lattice of  $\text{SiO}_2$  particles with diameter  $D=0.1\mu\text{m}$ .  $\sigma(u) = \sigma_0 u$ .  $\sigma_0=0.01$  for  $\eta=0.2$  and  $\eta=0.5$ .  $\sigma_0=0.001$  for  $\eta=0.9$ . Spacing (type *B*)  $s=1\mu\text{m}$  in the regular sequence (a). Spacings in the Fibonacci and Thue-Morse sequences of monolayers:  $s_{AA}=1\mu\text{m}$  for *AA*,  $s_{ABA}=2\mu\text{m}$  for *ABA* (b),(c), and  $s_{ABBA}=3\mu\text{m}$  for *ABBA* subsequences (c)

One can see that increasing the particle concentration in the monolayers leads to an increase in the depth and width of the PBGs. The spectral positions of the PBG minima are slightly shifted as well. The results also show the influence of the spacing between monolayers on the multilayer spectra. The spacing increase leads to an increase in the number of the

PBGs and their shifting to longer wavelengths. The PBGs relating to the Fibonacci and Thue-Morse sequences are typically narrower than the PBGs of the regular sequence, and the number of PBGs is larger.

Changing the particle concentration means changing the amount of material per unit area of a layer. For the plane-parallel homogeneous layer (plate), the amount of material per unit area is proportional to the plate thickness  $h$ .

Let us consider multilayers consisting of plane-parallel homogeneous layers with volume that is equal to the volume of particles in the monolayer sequences (their spectra are shown in Fig. 7). We will name such individual homogeneous layers as the equivalent plates. The thickness  $h$  of the equivalent plate is calculated as follows:

$$h = \frac{2}{3}\eta D, \quad (17)$$

where  $\eta$  is the filling coefficient of the monolayer of particles with diameter of  $D$ . The spectra of sequences consisting of homogeneous SiO<sub>2</sub> layers (type *A*) and air (type *B*) are displayed in Fig. 8. The amount of material in homogeneous SiO<sub>2</sub> layers is the same as in the particulate monolayers (Fig. 7).

Comparison of results for the particulate (Fig. 7) and homogeneous (Fig. 8) layers shows that with an increased amount of material in the layers, the depth and width of the PBGs increase. The PBGs of systems with homogeneous layers are typically wider and deeper than those of the particulate systems.

Now, let us calculate the spectra of the multilayer consisting of monolayers of particles with diameters equal to the thickness of the equivalent plate (see Fig. 8), i.e. when  $D = h_A$ . Figure 9 depicts the transmittance spectra of such a system consisting of the periodic (a), Fibonacci (b), and Thue-Morse (c) sequences of monolayers at  $\eta=0.9$ , which is close to the maximum value  $\eta_{\max} \approx 0.907$ .

The obtained results show that increasing the particle size leads to increases in the depth and width of the PBGs. The positions of PBGs in the spectra of the particulate systems are shifted to shorter wavelengths in comparison to those for homogeneous layer systems.

As follows from the results presented in Figs. 7-9, the PBGs in spectra for multilayers composed of homogeneous layers and of multilayers composed of particulate monolayers are different in their spectral positions, depths, and widths. The positions of PBGs in the spectra of the particulate structures are usually shifted to shorter wavelengths in comparison to those for homogeneous layers. Such a shift is larger for the aperiodic Thue-Morse sequence. The widths of the PBGs of the particulate systems are narrower than those for the homogeneous layer systems.

As one can see from Fig. 7 and Fig. 9, the Fibonacci and Thue-Morse sequences provide additional opportunities for spectrum manipulation in comparison with those for the regular sequence of monolayers. The layered particulate structures can be used in display applications, for creating multispectral lters, light emitting diodes, solar cells, etc.

### 3.5. Systems with small particles

As one can see from the results of Fig. 4c, the incoherent component of radiation of the partially-ordered monolayer is nonzero (i.e.  $T_c + R_c < 1$ ) for the considered monolayer parameters and the wavelength range. It is well known, that scattering by an individual small (relative to the wavelength of the incident light) dielectric particle decreases with decreasing particle size [48]. As a result, the intensity of radiation scattered by a monolayer of the sufficiently small dielectric particles tends to zero as well. In this case, the  $T_c$  and

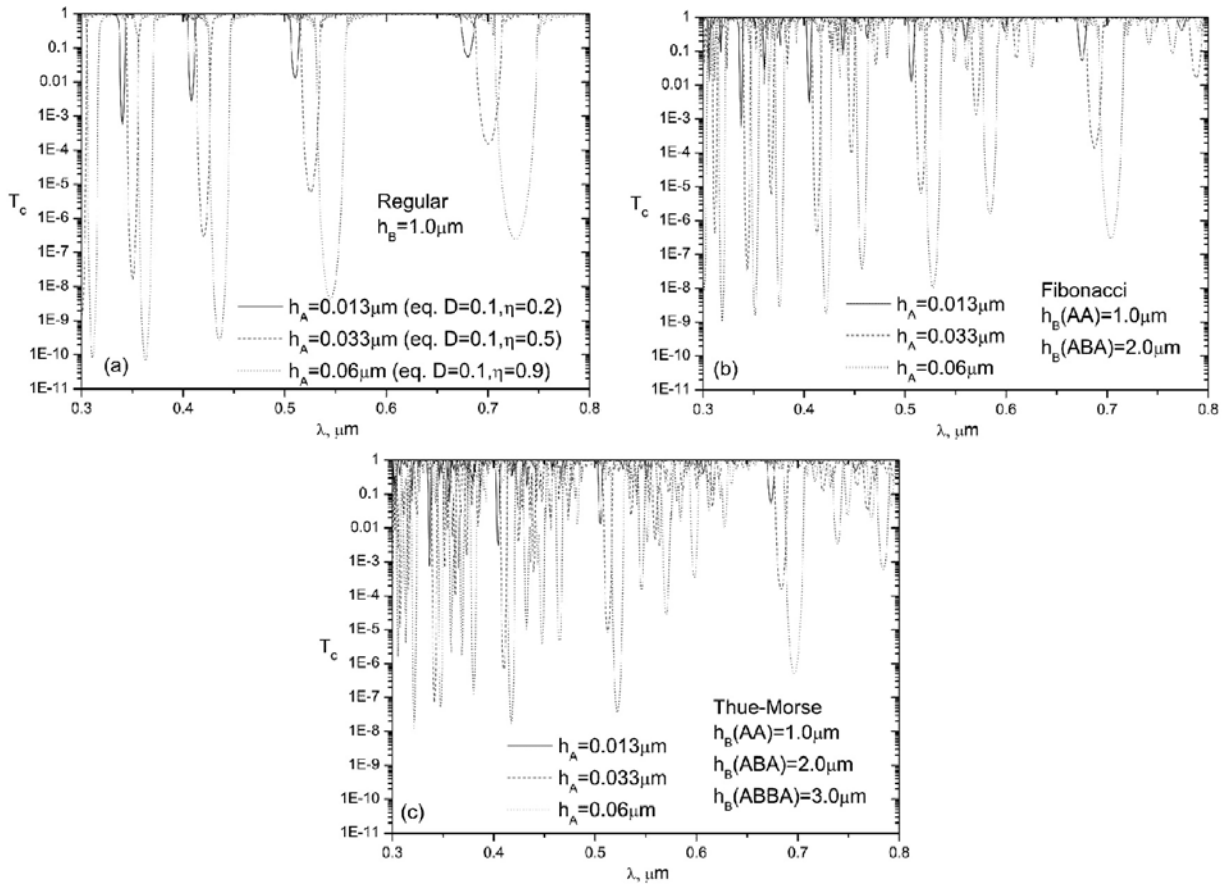


FIG. 8. Spectra of coherent transmission coefficient of the multilayer structures consisting of regular (a), Fibonacci (b), and Thue-Morse (c) sequences of homogeneous  $\text{SiO}_2$  layers (type A) and air (type B) at different thicknesses  $h_A$  of the layers. The number of  $\text{SiO}_2$  layers is 32. Spacing between the adjacent layers is  $h_B=1 \mu\text{m}$  for the regular sequence (a);  $h_B=1 \mu\text{m}$  for the AA,  $h_B=2 \mu\text{m}$  for ABA (b),(c), and  $h_B=3 \mu\text{m}$  for ABBA subsequences (c) in the Fibonacci and Thue-Morse sequences of layers

$R_c$  spectra of the individual partially-ordered and regularly-packed monolayers are nearly identical, and their  $T_c + R_c$  sums are practically equal to unity.

Let us consider the coherent transmission and reflection coefficients of monolayer sequences consisting of small particles. Figure 10 depicts the  $T_c$  and  $R_c$  spectra of the multilayer composed of the partially-ordered and the regularly-packed monolayers of  $\text{Al}_2\text{O}_3$  (type A) and  $\text{SiO}_2$  (type B) particles.

One can see that spectra of the multilayers consisting of the same sequences of the partially-ordered and regularly-packed monolayers of small particles are practically identical. Thus, optical response of multilayers consisting of monolayers of such particles is “insensitive” to the ordering in the individual monolayers.

#### 4. Conclusions

The developed technique reveals a good match with experiment [49] for the PBG position in the spectra of an artificial opal [50,51].

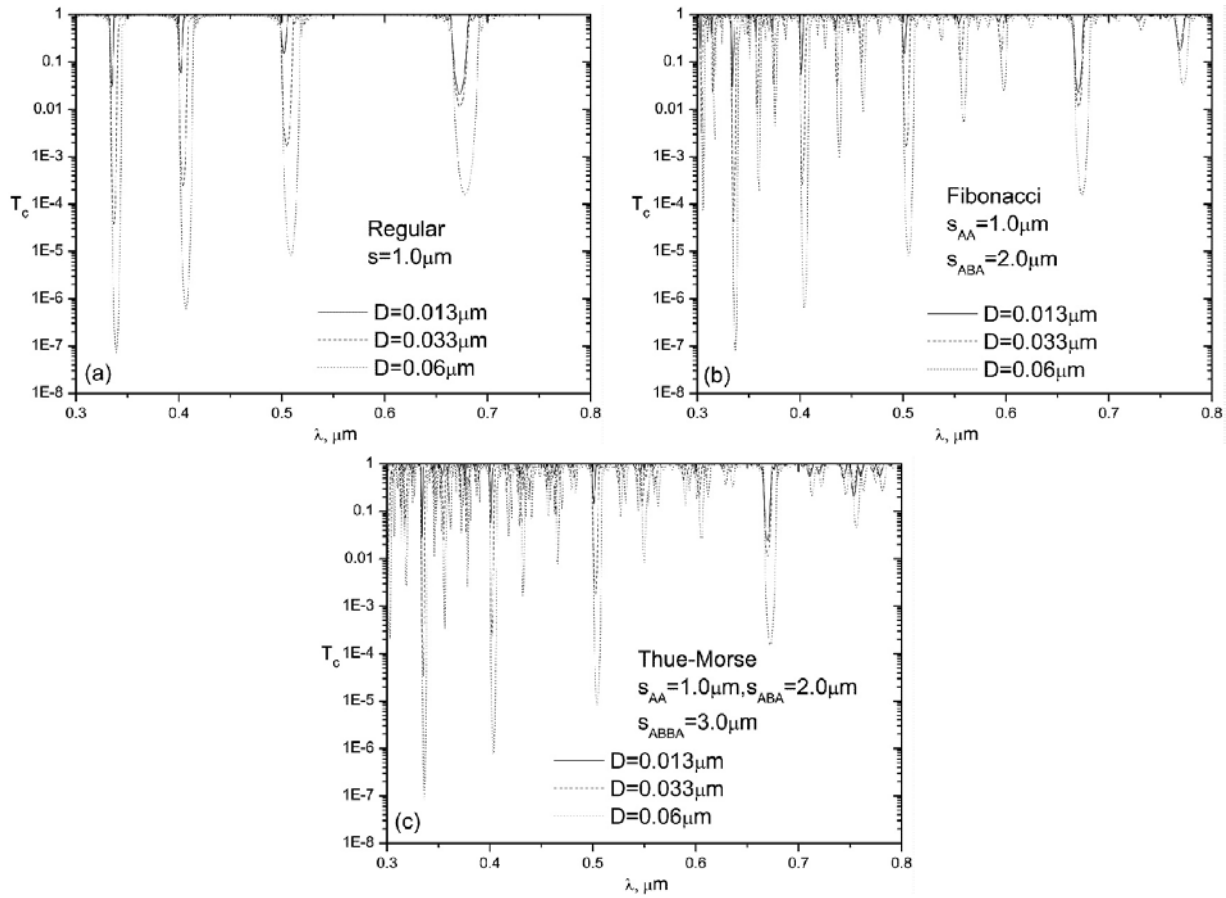


FIG. 9. Spectra of coherent transmission coefficient of the multilayer structures consisting of regular (a), Fibonacci (b), and Thue-Morse (c) sequences of 32 monolayers with triangular lattice of  $\text{SiO}_2$  particles at different diameters  $D$ . Filling coefficient of monolayers is  $\eta=0.9$ .  $\sigma(u)=\sigma_0u$ ,  $\sigma_0=0.001$ . Spacing between monolayers  $s=1\mu\text{m}$  in the regular sequence (a);  $s_{AA}=1\mu\text{m}$  for  $AA$ ,  $s_{ABA}=2\mu\text{m}$  for  $ABA$  (b),(c), and  $s_{ABBA}=3\mu\text{m}$  for  $ABBA$  subsequences (c) in Fibonacci and Thue-Morse sequences

The spectra of the coherent transmission and reflection coefficients of the layered structures consisting of periodic (regular), Fibonacci, and Thue-Morse sequences of  $\text{Al}_2\text{O}_3$  and  $\text{SiO}_2$  spherical particle monolayers are calculated. The quasicrystalline approximation for the individual monolayer and the transfer matrix method for the multilayer are used.

The influence of the number of monolayers on the transmission and reflection spectra of the multilayer is considered. It is shown quantitatively that the Fibonacci and Thue-Morse structures give additional opportunities to manipulate the spectrum of the multilayer in comparison to the regular ones. Unlike the spectra of the regular structures, the number of PBGs in the spectra of the Fibonacci and Thue-Morse multilayer structures increases with an increased number of monolayers.

It is shown that the PBG in the transmittance spectrum of the system consisting of two different types ( $A$  and  $B$ ) of monolayers is located in the wavelength range between the PBGs of the system consisting of only  $A$  type and of the system consisting of only  $B$  type monolayers.

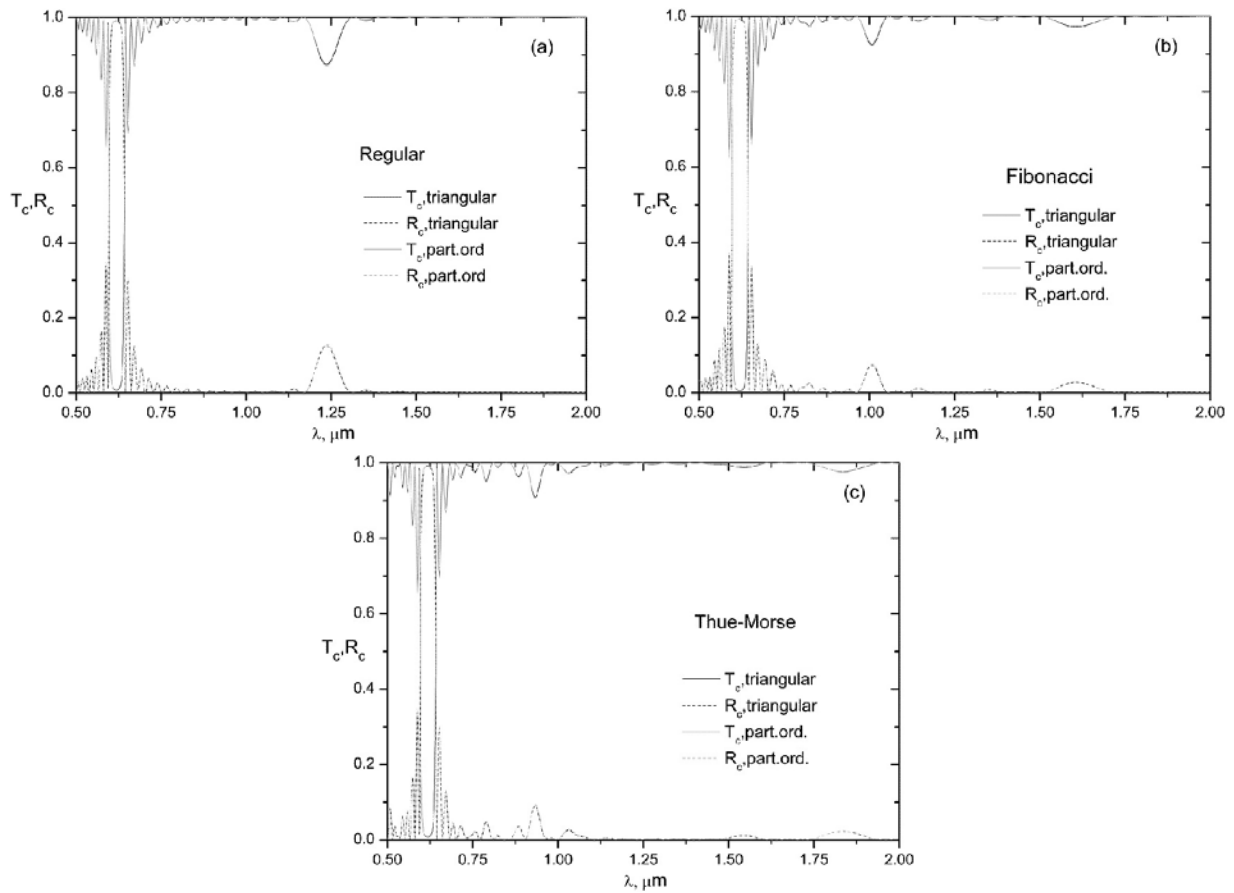


FIG. 10. Spectra of coherent transmission and reflection coefficients of a multilayer consisting of the regularly-packed (black lines) and partially-ordered (gray lines) monolayers of  $\text{Al}_2\text{O}_3$  (type A) and  $\text{SiO}_2$  (type B) particles. Monolayers are arranged in the regular (a), Fibonacci (b) and Thue-Morse (c) sequences. Number of monolayers is 34. Regularly-packed monolayers have a triangular lattice,  $\sigma(u) = \sigma_0 u$ ,  $\sigma_0 = 0.01$ .  $D = 0.05 \mu\text{m}$ ,  $\eta = 0.5$ ,  $s = 0.3 \mu\text{m}$

The spectra for multilayers consisting of homogeneous and particulate monolayers are compared. The PBGs of particulate structures are shifted to shorter wavelengths relative to those for structures consisting of homogeneous layers. The PBGs observed in the spectra for sequences of homogeneous layers are typically wider and deeper than those observed in the spectra of particulate systems.

The influence of particle concentration and spacing between monolayers on the spectra of the multilayer is studied. Increasing the concentration leads to growth in the depth, width, and wavelength of the PBG minima. Increasing the spacing between the monolayers leads to an increase in the number of PBGs and their shifting to longer wavelengths. These results can be used for the creation of multispectral filters based on layered particulate structures.

The coherent transmittance and reflectance for multilayers of regularly-packed and partially-ordered monolayers of small particles (in comparison with the wavelength of the incident light) are calculated. It is shown that their spectra are insensitive to the monolayer's ordering.

The obtained results can be used for the development of photonic band gap devices, multispectral filters, solar cells, light emitting diodes, display applications, etc.

## Acknowledgement

This work was supported in part by the state scientific and technical program of Belarus “Electronics and photonics”.

## References

- [1] I. A. Sukhoivanov, I. V. Guryev, *Photonic Crystals: Physics and Practical Modeling*, Springer-Verlag (2009).
- [2] J. D. Joannopoulos, S. G. Johnson, J. N. Winn, R. D. Meade, *Photonic Crystals: molding the flow of light*, Princeton: Princeton University Press (2008).
- [3] E. Yablonoitch, T. J. Gmitter. Photonic band structure: The face-centered-cubic case. *Phys. Rev. Let.*, **63**, P. 1950–1953 (1989).
- [4] D. Levine, P. J. Steinhardt. Quasicrystals: A New Class of Ordered Structures. *Phys. Rev. Let.*, **53**, P. 2477–2480 (1984).
- [5] D. Shechtman, I. Blech, D. Gratias, J. W. Cahn. Metallic Phase with Long-Range Orientational Order and No Translational Symmetry. *Phys. Rev. Let.*, **53**, P. 1951–1953 (1984).
- [6] H. Huang, C. H. Lin, Z. K. Huang, K. Y. Lee, C. C. Yu, and H. C. Kuo. Double Photonic Quasi-Crystal Structure Effect on GaN-Based Vertical-Injection Light-Emitting Diodes. *Jpn. J. Appl. Phys.*, **49**, P. 022101 (2010).
- [7] A. Ledermann, L. Cademartiri, M. Hermatschweiler, C. Toninelli, G. A. Ozin, D. S. Wiersma, M. Wegener, G. von Freymann. Three-dimensional silicon inverse photonic quasicrystals for infrared wavelengths. *Nat. Materials*, **5**, P. 942–945 (2006).
- [8] M. Florescu, S. Torquato, and P. J. Steinhardt. Designer disordered materials with large, complete photonic band gaps. *Proc. Natl. Acad. Sci.*, **106**, P. 20658–20663 (2009).
- [9] Sergei V. Zhukovsky, Andrei V. Lavrinenko, and Sergey V. Gaponenko. *Optical Filters Based on Fractal and Aperiodic Multilayers In Optics of Aperiodic Structures — Fundamentals and Device Applications*. Ed. by Luca Dal Negro, Springer, 509 p. (2013). P. 109–140.
- [10] A. Mouldi and M. Kanzari. Design of microwave devices exploiting Fibonacci and hybrid periodic/Fibonacci one dimensional photonic crystals. *Progress In Electromagnetics Research B*, **40**, P. 221–240 (2012).
- [11] R. W. Peng, M. Wang, A. Hu, S. S. Jiang, G. J. Jin, D. Feng. Photonic localization in one-dimensional k-component Fibonacci structures. *Phys. Rev. B*, **57**, P. 1544–1551 (1998).
- [12] L. Dal Negro and N.-N. Feng. Spectral gaps and mode localization in Fibonacci chains of metal nanoparticles. *Opt. Exp.*, **15**, P. 14396–14403 (2007).
- [13] P. W. Mauriz, M. S. Vasconcelos, E. L. Albuquerque. Optical transmission spectra in symmetrical Fibonacci photonic multilayers. *Phys. Let. A*, **373**, P. 496–500 (2009).
- [14] H. Aynaou, V. R. Velasco, A. Nougououi, E. H. El Boudouti, B. Djafari-Rouhani, D. Bria. Application of the phase time and transmission coefficients to the study of transverse elastic waves in quasiperiodic systems with planar defects. *Surface Science*, **538**, P. 101–112 (2003).
- [15] C. Sibilina, M. Bertolotti, M. Centini, G. D’Aguanno, M. Scalora, M. J. Bloemer, and Ch. M. Bowden. Linear and Nonlinear Optical Properties of Quasi-Periodic One-Dimensional Structures. in *Optical Properties of Nanostructured Random Media: Topics Appl. Phys.* **82**, V. M. Shalaev. ed. Springer-Verlag, Berlin, Heidelberg (2002), pp. 63–92.
- [16] C. Rockstuhl, F. Lederer, T. Zentgraf, H. Giessen. Enhanced transmission of periodic, quasiperiodic, and random nanoaperture arrays. *App. Phys. Let.*, **91**, P. 151109 (2007).
- [17] S. V. Boriskina, A. Gopinath, L. Dal Negro. Optical gap formation and localization properties of optical modes in deterministic aperiodic photonic structures. *Opt. Exp.*, **16**, P. 18813–18826 (2008).
- [18] Priya Rose T., E. Di Gennaro, G. Abbate, and A. Andreone. Isotropic properties of the photonic band gap in quasicrystals with low-index contrast. *Phys. Rev. B*, **84**, P. 125111-1 (2011).
- [19] L. F. Rojas-Ochoa, J. M. Mendez-Alcaraz, P. Schurtenberger, J. J. Saenz and F. Scheffold. Photonic properties of strongly correlated colloidal liquids. *Phys. Rev. Let.*, **93**, P. 073903 (2004).

- [20] M. Reufer, L. F. Rojas-Ochoa, P. Schurtenberger, J. J. Saenz and F. Scheffold. Transport of light in amorphous photonic materials. *Appl. Phys. Lett.*, **91**, P. 171904 (2007).
- [21] J. F. Galisteo-Lopez, M. Ibisate, R. Sapienza, L. S. Froufe-Prez, A. Blanco, C. Lopez. Self-assembled photonic structures. *Adv. Mater.*, **23**, P. 30–69 (2011).
- [22] C. Pouya, D. G. Stavenga, P. Vukusic. Discovery of ordered and quasi-ordered photonic crystal structures in the scales of the beetle *Eupholus magnificus*. *Opt. Exp.*, **19**, P. 11355 (2011).
- [23] O. Deparis, C. Vandembem, M. Rassart, V. Welch, J. P. Vigneron. Color-selecting reflectors inspired from biological periodic multilayer structures. *Opt. Exp.*, **14**, P. 3547–3555 (2006).
- [24] C. Campos-Fernández, D. E. Azofeifa, M. Hernández-Jiménez, A. Ruiz-Ruiz, W. E. Vargas. Visible light reflection spectra from cuticle layered materials. *Opt. Mater. Exp.*, **1**, P. 85–100 (2011).
- [25] C. C. Katsidis, D. I. Siapkas. General transfer-matrix method for optical multilayer systems with coherent, partially coherent, and incoherent interference. *Appl. Opt.*, **41**, P. 3978–3987 (2002).
- [26] E. Centurioni. Generalized matrix method for calculation of internal light energy flux in mixed coherent and incoherent multilayers. *Appl. Opt.*, **44**, P. 7532–7539 (2005).
- [27] M. C. Troparevsky, A. S. Sabau, A. R. Lupini, Z. Zhang. Transfer-matrix formalism for the calculation of optical response in multilayer systems: from coherent to incoherent interference. *Opt. Exp.*, **18**, P. 24715–24721 (2010).
- [28] M. Born, E. Wolf. *Principles of Optics. 7th ed.* Cambridge University Press (2002).
- [29] E. D. Palik, ed. *Handbook of optical constants of solids*. Academic (1985).
- [30] M. Lax. Multiple Scattering of Waves II. The effective field for dense systems. *Phys. Rev.*, **85**, P. 621–629 (1952).
- [31] K. M. Hong. Multiple scattering of electromagnetic waves by a crowded monolayer of spheres: application to migration imaging films. *J. Opt. Soc. Am.*, **70**, P. 821–826 (1980).
- [32] V. A. Loiko, A. A. Miskevich. Light propagation through a monolayer of discrete scatterers: analysis of coherent transmission and reflection coefficients. *Appl. Opt.*, **44**, P. 3759–3768 (2005).
- [33] A. A. Miskevich, V. A. Loiko. Two-dimensional planar photonic crystals: Calculation of coherent transmittance and reflectance at normal illumination under the quasicrystalline approximation. *JQSRT*, **112**, P. 1082–1089 (2011).
- [34] A. A. Miskevich, V. A. Loiko. Coherent transmission and reflection of a two-dimensional planar photonic crystal. *JETP*, **113**, P. 1–13 (2011).
- [35] L. L. Foldy. The multiple scattering of waves. *Phys. Rev.*, **67**, P. 107–119 (1945).
- [36] P. C. Waterman, R. Truell. Multiple scattering of waves. *J. Math. Phys.*, **2**, P. 512–537 (1961).
- [37] V. A. Babenko, L. G. Astafyeva, V. N. Kuzmin, *Electromagnetic scattering in disperse media*. Praxis Publishing Ltd (2003).
- [38] J. M. Ziman, *Models of Disorder*. Cambridge University (1979).
- [39] Z. Fisher. *Statistical Theory of Liquids*. University of Chicago Press (1964).
- [40] D. A. Varshalovich, A. N. Moskalev, V. K. Khersonskii, in *Quantum theory of angular momentum*. Singapore: World Scientific (1988). Original Russian edition: Leningrad: Nauka (1975).
- [41] J. P. Mondia, Tan Hong Wee, S. Linden, H. M. van Driel, J. F. Young. Ultrafast tuning of two-dimensional planar photonic-crystal waveguides via free carrier injection and the optical Kerr effect. *J. Opt. Soc. Am. B*, **22**, P. 2480–2486 (2005).
- [42] M. Devetak, J. Milavec, R. A. Rupp, B. Yao, I. Drevenšek-Olenik. Two-dimensional photonic lattices in polymer-dispersed liquid crystal composites. *J. Opt. A: Pure Appl. Opt.*, **11**, P. 024020 (2009).
- [43] Y. Kurokawa, Y. Jimba, H. Miyazaki. Internal electric-field intensity distribution of a monolayer of periodically arrayed dielectric spheres. *Phys. Rev. B*, **70**, P. 155107 (2004).
- [44] L. S. Ornstein, F. Zernike. Accidental deviations of density and opalescence at the critical point of a single substance. *Proc. Acad. Sci.*, **17**, P. 793–806 (1914).
- [45] J. K. Percus, G. J. Yevick. Analysis of classical statistical mechanics by means of collective coordinates. *Phys. Rev.*, **110**, P. 1–13 (1958).
- [46] A. P. Ivanov, V. A. Loiko, V. P. Dick. *Propagation of light in close-packed disperse media*. Minsk: Nauka i Tekhnika (1988) (in russian).
- [47] V. A. Loiko, A. V. Konkolovich. Spatial Optical Noise of a Monolayer of Discrete Inhomogeneities: I. Basic Relations for the Wiener Spectrum. *Optics and spectroscopy*, **85**(4), P. 563–567 (1998).
- [48] H. C. van de Hulst. *Light Scattering by Small Particles*. Dover Publications (1981).

- [49] V. N. Bogomolov, S. V. Gaponenko, I. N. Germanenko, A. M. Kapitonov, E. P. Petrov, N. V. Gaponenko, et al. Photonic band gap phenomenon and optical properties of artificial opals. *Phys. Rev. E*, **55**, P. 7619–7625 (1997).
- [50] V. A. Loiko, A. A. Miskevich. Coherent Transmission and Reflection Spectra of Ordered Structures from Spherical Alumina Particles. *Opt. and Spectrosc.*, **115**, P. 274–282 (2013).
- [51] A. A. Miskevich, V. A. Loiko. Layered periodic disperse structures of spherical alumina particles: Coherent transmittance and reflectance spectra. *JQSRT* (2013), <http://dx.doi.org/10.1016/j.jqsrt.2013.05.013>.